

1 **Title:** Drone data reveal heterogeneity in tundra greenness and phenology not captured by
2 satellites

3

4 **Authors:** Jakob J. Assmann¹, Isla H. Myers-Smith², Jeffrey T. Kerby³, Andrew M. Cunliffe⁴,
5 Gergana N. Daskalova²

6

7 **Affiliations:** ¹ Department of Biology, Aarhus University, DK

8 ² School of GeoSciences, University of Edinburgh, UK

9 ³ Aarhus Institute of Advanced Studies, Aarhus University, DK

10 ⁴ Department of Geography, University of Exeter, UK

11

12 **ORCID:** Jakob J. Assmann: 0000-0002-3492-8419

13 Isla H. Myers-Smith: 0000-0002-8417-6112

14 Jeffrey T. Kerby: 0000-0002-2739-9096

15 Andrew M. Cunliffe: 0000-0002-8346-4278

16 Gergana Daskalova: 0000-0002-5674-5322

17

18 **Abstract:**

19

20 Data across scales are required to monitor ecosystem responses to rapid warming in the
21 Arctic and to interpret tundra greening trends. Here, we tested the correspondence among
22 satellite- and drone-derived seasonal change in tundra greenness to identify optimal spatial
23 scales for vegetation monitoring on Qikiqtaruk - Herschel Island in the Yukon Territory,
24 Canada. Combining time-series of the Normalised Difference Vegetation Index (NDVI) from
25 ultra-fine-grain multispectral drone imagery and satellite data (Sentinel-2 and MODIS) with
26 ground-based observations for two growing seasons (2016 and 2017), we found high
27 cross-dataset correspondence in peak season greenness (Spearman's $\rho > 0.77$) and
28 cross-season greenness changes (drone-sentinel $R^2 = 0.69$) for eight one-hectare plots, with
29 drones capturing lower NDVI values relative to Sentinel-2 satellites. We identified a plateau
30 in the spatial variation of tundra greenness at distances of around half a metre in the plots,
31 suggesting that these grain sizes are optimal for monitoring such variation in the two most
32 common vegetation types on the island. We further observed a notable loss of seasonal
33 variation in the spatial heterogeneity of landscape greenness (46.2 - 63.9%) when
34 aggregating from ultra-fine-grain drone pixels (approx. 0.05 m) to the size of medium-grain
35 satellite pixels (10 – 30 m). Finally, seasonal changes in drone-derived greenness were
36 highly correlated with measurements of leaf-growth for focal deciduous species in the
37 ground-validation plots (mean Spearman's $\rho = 0.68$). These findings indicate that
38 multispectral drone measurements can capture temporal plant growth dynamics across
39 tundra landscapes. Overall, our results demonstrate that novel technologies such as drone
40 platforms and compact multispectral sensors allow us to study ecological systems at
41 previously inaccessible scales and fill gaps in our understanding of tundra ecosystem
42 processes. Capturing fine-scale variation across tundra landscapes will improve predictions
43 of the ecological impacts and climate feedbacks of environmental change in the Arctic.

44

45 **Keywords:** Arctic tundra, vegetation monitoring, landscape phenology, satellite, drones,
46 UAV and RPAS, NDVI, scale

47 Introduction

48

49 Identifying the scales at which ecological processes operate is a fundamental, yet often
50 neglected element of ecological research (1–3). Cross-scale ecological information can
51 inform our understanding of the causes and consequences of global change (2). In tundra
52 ecosystems, vegetation responses triggered by rapid Arctic warming could influence
53 ecosystem functions through altered carbon and nutrient cycles with potential feedbacks to
54 the global climate system (4–8). Yet, challenging logistics have limited the extent of
55 field-based observations in Arctic ecosystems (9–11). The grain sizes of global-extent
56 satellite products (tens of meters to kilometres) are too coarse to capture the fine-scale
57 dynamics of tundra plants (12–14) and to link vegetation change to key ecosystem functions
58 (13). Thus by bridging this “scale-gap”, we can transform our understanding of pan-Arctic
59 tundra vegetation change and associated global-scale climate feedbacks.

60

61 *Satellites show greening of the tundra*

62

63 Satellite observations indicate a ‘greening’ of tundra ecosystems (13,15–20) and shifts in
64 growing season phenology over recent decades (13,21–24). Observations of increasing
65 tundra greenness are often reported from surface-reflectance-derived Normalised Difference
66 Vegetation Index (NDVI) (13,16,25,26). Satellite-observed tundra greening has been
67 concurrent with ground-based observations of vegetation change in Arctic ecosystems (27)
68 including increasing shrub cover (28–31) and taller community level plant height (32), as well
69 as earlier leaf emergence and flowering at some (33–36), but not all tundra sites (37–39).
70 However, mismatches between ground and satellite-based observations suggest the
71 potential for an observational scale gap (13).

72

73 *Arctic vegetation change and phenology have been linked to warming*

74

75 Satellite-observed Arctic greening trends have been linked directly to warming air
76 temperatures (13,19,20,40–46) and indirectly to sea-ice declines (17,47–51). Ground-based
77 observations of tundra vegetation change correspond with warming (27,32,52) but do not
78 always co-occur with satellite greening trends in the regions around the ecological
79 monitoring sites (13,53). While satellite-based phenology observations from the Arctic have
80 been mainly linked to temperature (22,54,55), *in situ* phenology in the tundra has been
81 shown to be influenced by a suite of interacting factors including, but not limited to:
82 snowmelt, temperature, day length, and the proximal influences of sea-ice on localised
83 climate affect (34–36,38,56,57). Thus, ecological studies indicate greater complexity of
84 drivers that analyses of satellite-derived greening trends to date.

85

86 *Inconsistencies amongst satellite platforms and heterogenous greening trends*

87

88 Greening trends and phenology measures derived from different satellite platforms do not
89 always correspond (13,18) and greening trends vary at global (18), continental (42,58–60)
90 and regional scales (46–48,61–64). Many areas of the Arctic show no trends in NDVI, with
91 only around 20% of the Arctic spectrally greening and around 1 - 4% of the Arctic spectrally
92 browning (13,62,65,66). Recent analyses suggest a slowdown of the Arctic-wide spectral

93 greening trend over the past decade (43,67). Furthermore, despite NDVI being related to the
94 photosynthetically active biomass in the tundra (14,68–70), geophysical, environmental and
95 ecological factors, in addition to the non-linearity of NDVI-biomass relationships, complicate
96 the interpretation of satellite-derived NDVI time-series at high-latitudes (13,71). The growing
97 complexity highlighted in Arctic greening trends has led to repeated calls for ground
98 validation of satellite observations (11,13,18,59,60,66,72,73).

99

100 *The scale discrepancy problem in Arctic greening*

101

102 A major problem in linking satellite-derived trends of tundra spectral greenness and
103 phenology to *in situ* observations of ecological processes is the discrepancy in observational
104 scales (13,29,61,72,74). Satellite datasets with long-term records are limited by their
105 moderate- to coarse-grain sizes, ranging from 30 m (Landsat) to 250 m (MODIS) and 8 km
106 (AVHRR-GIMMS3g). *In situ* ecological monitoring in the Arctic is logistically challenging and
107 therefore restricted in extent to a limited number of sites and often metre-squared plots
108 (10,75). Only a few studies have linked on-the-ground vegetation or phenology change to
109 satellite trends in NDVI in Arctic tundra (13,14,47,48,53,76–78). However, drones equipped
110 with compact sensors now allow for the collection of ultra-fine-grain multispectral imagery at
111 landscape extents that can potentially bridge the scale-gap between satellite and
112 ground-based observations (14,79–82).

113

114 *Novel drone data to study variation in greenness*

115

116 Here, we set out to test whether drones can be used to identify the key ecological scales for
117 studying tundra greenness on Qikiqtaruk by bridging the scale gap between satellite and *in*
118 *situ* data. First, we tested whether satellite- and drone-derived measures of mean
119 landscape-scale greenness (NDVI) agree across two growing seasons while controlling for
120 the potentially confounding effects of topography and land cover. Second, we identified the
121 key spatial scales for ecological variation in landscape greenness within the two most
122 common vegetation types at our study site using variograms. Third, we tested how the
123 magnitude of seasonal variation in tundra greenness scales across grain sizes from
124 fine-resolution drone imagery to medium-grain satellite imagery. Finally, we assessed
125 whether drone-derived NDVI corresponds with on-the-ground measures of within growing
126 season change in plant growth frequently measured by long-term field-based monitoring
127 networks. Thus, in our analysis we validated satellite-derived landscape estimates of
128 vegetation greenness with ultra-fine-grain drone data and described spatial and temporal
129 variation in tundra productivity at grain sizes and extents that were not previously accessible.

130

131 **Methods**

132

133 *Site description: Qikiqtaruk - Herschel Island*

134

135 Qikiqtaruk (69.57 N, 138.91 W) is located in the Beaufort Sea along the coastline of the
136 North Slope of the Yukon Territory, Canada. The vegetation is characteristic moist acidic
137 shrub tundra (83) found in the Western Arctic regions of North America that has experienced
138 strong spectral greening in recent decades (13). The two most common plant communities

139 on the island are the tussock sedge (“Herschel”) and Dryas-vetch (“Komakuk”) vegetation
140 types (84,85). We established four study areas on the east end of the island, each with two
141 co-located one-hectare plots in the two key vegetation cover types (Figure 1, Table S1). We
142 selected plots with homogenous terrain and land cover to represent the two key vegetation
143 types and to control for the potentially confounding effects of terrain and cover heterogeneity.

144

145 *Multispectral drone time-series*

146

147 We analysed 62 drone surveys across four research areas with one-hectare plots in the two
148 vegetation types at the site (Table S3). We collected multispectral drone imagery using
149 Parrot Sequoia (Paris, France) compact multispectral sensors mounted on multi-rotor drone
150 platforms in June to August in 2016 and 2017. We used three different drone platforms: a
151 Tarot 680 Pro hexacopter with camera sensor stabilisation in 2016, and a 3DR Iris+ and a
152 DJI Phantom 4 Pro without sensor stabilisation in 2017. Surveys were flown in a lawn-mower
153 flight pattern at an altitude of ca. 50 m, giving ground-sampling distances of 0.04 m to 0.06
154 m. Images were acquired with 75% front- and side-lap as close as possible to solar noon
155 (mean absolute difference to solar noon 2.16 h, maximum 6-7 h). See Table S3 for further
156 details.

157

158 We processed the Sequoia imagery using Pix4D Mapper v4.0.21 (Lausanne, Switzerland)
159 with the *agMultispectral* template and the ‘merge map tiles’ option set to true to generate
160 co-registered single-band surface reflectance maps. Radiometric calibration was carried out
161 in Pix4D Mapper using pre- or post-flight imagery of calibrated reflectance panels; in 2016
162 we used a MicaSense (Seattle, USA) panel and in 2017 a SphereOptics (Herrsching,
163 Germany) Zenith Lite panel. We measured panel reflectance pre- and post- season and
164 used the mean values for radiometric calibration. We also calibrated for sensor properties
165 and sun irradiance measured by the incident light sensor. We used four to six ground control
166 points per survey to geolocate the imagery in Pix4D Mapper with an estimated accuracy of
167 1-2 pixels between bands and 2-6 pixels between surveys (81). We calculated the Sequoia
168 NDVI as the normalised difference between the near-infrared (770 nm – 810 nm) and red
169 (640 nm – 680 nm) bands of sensor.

170

171 *Satellite time-series*

172

173 We obtained MODIS NDVI values for the time period between May and September 2016
174 and 2017 for all 250 m MODIS pixels that contained the survey plots. NDVI values were
175 retrieved from the 16-day MOD13Q1 v6 Terra product (86) using the Google Earth Engine
176 (87). We discarded all values with a ‘Summary QA’ score of -1 (no data) or 3 (cloudy). Table
177 S4 lists the resulting MODIS-pixel-date pairs. The MODIS NDVI is calculated as the
178 normalised difference between bands 1 (841 nm – 876 nm) and band 2 (620 nm – 670 nm).

179

180 For the Sentinel-2 time-series, we gathered all Sentinel-2 MSI L1C scenes containing the tile
181 covering Qikiqtaruk (T07WET) that were available on the Copernicus Open Access Hub
182 (<https://scihub.copernicus.eu/>) for the same time period as the MODIS pixels. We processed
183 all scenes to L2A using Sen2Cor 2.4.0 (88), retained all bands with 10 m resolution (2-4 &
184 8), applied the cloud mask and generated a true-colour image. We inspected all scenes

185 visually and discarded all imagery with cloud contamination over the study area (78% of
186 scenes for 2016 and 74% of scenes for 2017). The resulting set contained nine cloud-free
187 Sentinel-2 L2A scenes of the study area from 2016 and fifteen scenes from 2017 (Table S5).
188 Finally, the Sentinel NDVI was calculated as the normalised difference between band 8
189 (784.5 nm - 899.5 nm) and band 4 (650 nm - 680 nm).

190

191 *Ground-based plant phenology measurements*

192

193 We carried out ground-based phenology monitoring in eight 2 m x 2 m plots (Table S2), one
194 adjacent to each one-hectare plot (mean distance = 23 m, max distance = 52 m). Within
195 these plots we monitored six individual plants from the most common species: *E. vaginatum*,
196 *D. integrifolia*, *S. pulchra* and *A. latifolia* in tussock sedge tundra; *D. integrifolia*, *S. arctica*
197 and *A. latifolia* in Dryas-vetch tundra. We measured the length of the longest leaf on each
198 individual on the survey date to the nearest millimetre. This approach is widely used in
199 field-based phenology monitoring protocols (89), and will allow for NDVI to be directly related
200 to phenological changes in plant traits. The majority of ground-based phenology surveys
201 were carried out on the same day as the drone surveys (mean difference = 0.3 days,
202 maximum difference = 3 days, Table S6).

203

204 *Cross-sensor correspondence*

205

206 To test cross-sensor correspondence, we first plotted the mean NDVI for all plots,
207 time-points and sensors available (MODIS = single pixel) across both growing seasons. We
208 then calculated the mean difference and Spearman's rank correlation of the peak-season
209 NDVI for 2017 amongst the sensors (mean 20 July - 10 August). We matched all drone and
210 Sentinel-2 scenes that were less than two days apart, resampled the drone bands to the
211 Sentinel-2 grid, calculated the NDVI and tested the predictive relationship between the
212 resampled drone and sentinel NDVI pixel-pairs for a random sub sample (10% of total, n =
213 700) with Bayesian linear models (Table S9 and S10) from the MCMCglmm v.2.29 package
214 (Hadfield 2010).

215

216 *Spatial autocorrelation*

217

218 To assess the spatial autocorrelation of variation in tundra greenness within the eight plots,
219 we sampled variograms and fitted variogram models using the gstat v. 2.0-5 package
220 (Pebesma 2004, Gräler et al 2016). All variograms were sampled with a bin width of 0.15 m
221 from 0 to 15 m and a bin width of 3 m from 0 to 45 m.

222

223 *Grain size and phenology*

224

225 We tested the influence of grain-size on observations of tundra greenness phenology by
226 fitting simplified growing season curves to the raster stacks for each plot and season. We
227 first resampled the drone bands for all time-points to grids with grain sizes of 0.5, 1, 5, 10, 20
228 and 33.33 m. We then calculated the NDVI and fitted simple quadratic models to each pixel
229 in the growing season stacks ($y = ax^2 + bx + c$, where x is the day of year and y the pixel
230 NDVI, a the quadratic coefficient, b the linear coefficient and c the constant term). We found

231 a strong negative correlation between the quadratic and linear coefficients of the models
232 (Figure S5), we selected only the quadratic coefficient for further analysis.

233

234 *Ground validation*

235

236 To test the correspondence between our ground-based phenology measurements and the
237 drone observations, we derived time-series of the mean longest leaf length and greenness
238 for each 2 m x 2 m ground-based monitoring plot. For each drone survey, we calculated the
239 mean-NDVI of the 2 m x 2 m monitoring plot and matched this with the mean longest leaf
240 length values derived from the corresponding ground-based surveys (Table S6). We then
241 calculated the Spearman's rank correlation between mean-NDVI and mean longest feaf
242 length for each plot and season.

243

244 *Statistical analyses*

245

246 We conducted statistical analyses using R v. 3.6.0 (90). We used the 'resample' function of
247 the raster package in R for resampling from finer to coarser resolutions (91). See extended
248 methods for further information.

249

250 **Results**

251

252 *Landscape greenness corresponded among sensors*

253

254 Landscape greenness corresponded among drone, Sentinel-2 and MODIS across both the
255 2016 and 2017 growing seasons. Growing season curves of the plot mean NDVI were
256 similar (Figure 1) and peak-season plot mean NDVI values for 2017 were highly correlated
257 across sensors (Spearman's $\rho > 0.77$, Table S7). However, we observed an offset between
258 drone and satellite plot-mean NDVI of around 0.08 absolute NDVI that was consistent for
259 both MODIS and Sentinel platforms (Table S8). Resampled 10 m drone pixels and the
260 corresponding spatially co-located Sentinel-2 pixels were highly correlated (marginal $R^2 =$
261 0.69, see Figure 2 and Table S9). We found that vegetation type, the specific Sentinel
262 platform (Sentinel-2A / Sentinel-2B), and the time-difference between Sentinel scene and
263 drone data acquisition influenced the relationship between Sentinel-2 pixel NDVI and
264 drone-derived NDVI (marginal $R^2 = 0.87$, Table S10).

265

266 *Spatial variation in landscape greenness peaked at approx. 0.5 m*

267

268 We observed a peak in spatial variation in the NDVI values of pixel pairs for distances below
269 0.5 meter (mean range 0.46 m) during the peak-season of 2017 (26-28 July) and little
270 additional spatial variation was found between pixel pairs for distances of up to 45 m
271 thereafter (Figure 3). This pattern was consistent across vegetation types in seven out of our
272 eight plots (Figure 3, S2 and S3). The only exception is the Dryas-vetch plot in Area 3, which
273 showed the same patterns for distance below 10 m, but thereafter spatial variation steadily
274 increased (Figure S3).

275

276 *Seasonal-variation was lost when aggregating to medium grain sizes*

277

278 We observed a notable loss in the amount of seasonal variation in tundra greenness when
279 aggregating grain size from ultra-fine-grain drone to medium-grain satellite data. The loss
280 was particularly pronounced at grain-sizes above 10 m – the grain size of Sentinel-2 MSI
281 pixels (46.2 - 63.9%) (Figure 4). The variation in the quadratic coefficient of the simple
282 growing season curves (Figure 4b and S6) decayed logarithmically with grain size (Figure
283 4a), while no change occurred in the mean tendency of the coefficient (Figure S4). The
284 quadratic and linear coefficients of the growing season curves were strongly correlated
285 (Spearman's $\rho = -0.999$), thus the same pattern holds true for the linear component of the
286 curve fit (Figure S5).

287

288 *Drone-derived spectral greenness correlated well with leaf measurements*

289

290 Drone-derived spectral greenness correlated well (mean $\rho = 0.66 - 0.71$) with ground-based
291 measurements of cross-season phenology for graminoids and deciduous plants (Figure 5).
292 The mean Spearman's correlation coefficient of the measured mean leaf length and the
293 mean NDVI values in the ground-based phenology plots was 0.68 across all species and
294 time-series (Table S11 and Figure 5a). The graminoids and deciduous shrub species
295 followed this mean tendency well across all time-series, while the partially-evergreen *D.*
296 *integrifolia* showed mixed responses between plots and years (mean $\rho = 0.22$, Figure 5a).
297 The drone-based greenness time-series of the 2 m x 2 m ground-phenology plots highlight
298 fine-scale differences in phenology such as the continuous greening of tussocks that was
299 visible at the tussock sedge tundra plot in Area 2 (Figure 5c).

300

301 **Discussion**

302

303 Our analysis of cross-scale time-series of landscape greenness on Qikiqtaruk highlights four
304 main findings: 1) Measures of mean tendency in landscape greenness were consistent, but
305 slightly offset with drones capturing lower NDVI values than Sentinel-2 and MODIS satellites
306 (Figures 1 and 2). 2) The majority of variation in landscape greenness was contained at
307 scales of around half-a-metre, and thus not captured by medium-grain satellites such as
308 Sentinel-2 (Figure 3). 3) When aggregating growing season curves from ultra-fine-grain
309 drone to medium-grain satellite pixel sizes, a notable amount (46.2 - 63.9%) of variation in
310 greenness phenology was lost (Figure 4). 4) Drone-based measures of landscape greenness
311 correlated well with ground-based measurements of leaf length (Figure 5). Taken together,
312 our results highlight that drone platforms and compact multispectral sensors can capture key
313 ecological processes such as vegetation phenology and bridge the existing scale gap
314 between satellite and ground-based monitoring in tundra ecosystems.

315

316 Our study indicates cross-platform agreement, yet a positive offset, in mean landscape
317 greenness. The correspondence between drone and satellite-derived NDVI has yet to be
318 tested across Arctic sites (13,14). Some studies of natural or agricultural systems have
319 reported similar or higher levels of agreement between multispectral reflectance products
320 from drones and satellites (14,92,93), while others reported mixed or poor agreement
321 (94–96). As in Franzini et al. (2019), we observed a positive offset between drone and
322 satellite NDVI (Figure 2a and Table S8) that warrants further investigation. Possible

323 ecological interpretations of this offset are that drone data better capture low NDVI values.
324 Possible technical explanations for this offset include: differences in viewing geometries
325 between drones (highly variable) and satellites (relatively consistent), distinct sensor
326 properties of drone and satellite sensors, influences of the atmosphere between the sensor
327 and the land surface and a variety of other factors influencing the estimated reflectance.
328 Siewert and Olofson (2020) do not report this offset in the more heterogenous tundra of
329 Arctic Sweden, raising the possibility that within-landscape variation in land cover or
330 topography may influence correspondence between vegetation greenness across scales.
331 The homogeneity of the landscape within our survey plots likely contributes to the strong
332 correlation between drone- and satellite-derived NDVI that we have observed (13).
333 Additional research is needed to evaluate how other scale-varying landscape characteristics
334 like land cover (including non-vegetative surfaces like water, rocks, snow, etc.) and
335 topography affect drone and satellite correspondence across the diverse and structurally
336 complex tundra biome.

337

338 In our study, ecological information was lost when upscaling from ultra-fine-grain (~ 0.05 m)
339 drone to moderate grain (~ 10 – 30m) satellite resolutions. Even the most recent generation
340 of freely-available multispectral satellite products can be limited in their ability to capture
341 fine-grain ecological processes of tundra vegetation change (13). Information transfer during
342 upscaling leads to the loss of more information in tundra ecosystems compared to other
343 biomes (14,97) as land cover and vegetation structure are fragmented at finer scales (98).
344 However, exactly how spatial aggregation influences the loss in observed ecological
345 variability across the diversity of Arctic landscapes remains poorly quantified (11,13). Yet,
346 this variability is critical to understanding climate-driven changes in vegetation phenology
347 (35,36,99), plant-pollinator interactions (100), and trophic interactions (101). With
348 drone-based monitoring, we observed a decrease in magnitude of the spatial variability in
349 landscape-level phenology throughout the growing season (Figures 4 and Figure S2), while
350 aggregation to moderate satellite grains obscured both the magnitude and timing of
351 phenological heterogeneity (Figures 4 and S6). Thus, time-series of fine-grain
352 remotely-sensed observations will be critical for answering key research questions about
353 tundra ecosystem functioning in a warming Arctic (102).

354

355 Our results indicate that drone-based greenness time-series captured variation in plot-level
356 leaf-growth of deciduous tundra plant species. We demonstrate how drones can be used to
357 measure variation in tundra plant phenology of metre-scale patches at landscape extents.
358 Drones have been successfully used to monitor phenology of individual plants (trees) in
359 temperate forest ecosystems (103–105), and our study indicates that individual plant-level
360 phenology monitoring of sub-decimeter variability from drones could also be carried out in
361 tundra ecosystems. Future studies that quantify plant growth or phenology events such as
362 leaf emergence and flowering across the landscape could provide key information on
363 resource availability for plant-consumer interactions (100,101). Our findings also highlight
364 known limitations of NDVI to track phenology in evergreens or other non-deciduous taxa (*D.*
365 *integrifolia*, Figure 5), suggesting that tests of alternative vegetation index - plant growth
366 relationships (105) are needed to capture cross-season variation in tundra evergreen and
367 moss species. Combining drone-based time-series with observations from phenocams,
368 satellite and ground-based study plots has the potential to revolutionise our understanding of

369 landscape-scale phenology (13) by moving beyond the previously small samples of
370 individuals monitored in the Arctic tundra (36,37,39,106).

371

372 Our study highlights limitations and challenges associated with the collection of multispectral
373 drone time-series in Arctic ecosystems. Recent studies have discussed challenges
374 associated with the use of compact multispectral drone sensors including radiometric
375 consistency and repeatability (81,107,108). Due to logistic constraints, we were not able to
376 always conduct surveys under optimal conditions due to sun angle or cloud cover nor as
377 frequently as planned due to wind or precipitation (Table S3), which likely introduced bias
378 and/or noise into our drone data (e.g., Figure 4b). Access limitations meant that we could not
379 capture spring and autumn on Qikiqtaruk. As an early-generation multispectral drone sensor,
380 the Parrot Sequoia was tailored for deriving the NDVI, which despite being the legacy
381 workhorse of tundra remote-sensing has limitations (11,13). In particular, NDVI can be
382 confounded by moisture and surface water (11,13,73,109), complicating interpretation in wet
383 tundra and particularly in fine-grain size data. However, the rapid technological development
384 of drones and sensors, as well as further consolidation and standardisation of methods
385 (110), will allow for pan-Arctic syntheses of fine-grain data to resolve the uncertainty and
386 complexity of Arctic greening patterns trends (13,14,81) (see also the High Latitude Drone
387 Ecology Network - <https://arcticdrones.org/>).

388

389 Our study demonstrates that drones can fill the scale-gap between satellite and field studies
390 in the observation of terrestrial Arctic vegetation change (13,111). Rather than investigating
391 and explaining patterns at scales pre-defined by satellite datasets or field-based networks,
392 researchers can use drones to identify scale-domains that are most closely associated with
393 ecological processes of interest. Field ecologists can now use scaling theory provided by the
394 remote sensing community (74,112–115) at scales and temporal intervals that will allow for
395 hypothesis testing about what mechanisms are driving landscape-level ecological change.
396 Drone imagery will also allow the remote sensing community to track the effects of sub-pixel
397 heterogeneity on satellite products down to the grain of individual plants and communities
398 (14) that have been long studied by field-based monitoring networks, like the International
399 Tundra Experiment (75). Only by improving our understanding of how ecologically important
400 information is captured across grain sizes can we reduce uncertainties in the medium- and
401 coarse-grain satellite observation that feed into Earth system models and shape their
402 predictions (4,8). Fine-scale remote sensing from drones and aircraft provides key tools for
403 disentangling the drivers behind the greening of the Arctic (13,14,79,102).

404

405 **Conclusions**

406

407 Novel remote-sensing technologies such as drones now allow us to study ecological
408 variation in landscapes continuously across scales. Fine-grain ecological observation is of
409 particular importance where variation in plant growth happens at very small spatial scales
410 such as in tundra ecosystems (13,71). Our finding of a peak in spatial variation found at
411 distances of ~0.5 m in the plots on Qikiqtaruk shows the grain size at which phenological
412 information within the plant communities is best captured at this site. We demonstrate that
413 key ecological information is lost when observing the tundra at even decimeter or coarser
414 scales, such as those of medium grain satellites (~ 10 – 30m). Despite the methodological

415 challenges of collecting multispectral drone imagery in remote environments (81), our
416 time-series of vegetation greenness correlated well with ground-based measurements of leaf
417 growth in the validation plots. Drones now enable cross-scale studies that fill scale gaps
418 between satellite and ground-based observations facilitating the identification of key drivers
419 of vegetation change to inform projections of climate change impacts and feedbacks in the
420 tundra biome.

421

422 **Acknowledgements**

423

424 We would like to thank the Team Shrub field crews of the 2016 and 2017 field seasons for
425 their hard work and effort invested in collecting the data presented in this research, this
426 includes Will Palmer, Santeri Lehtonen, Callum Tyler, Sandra Angers-Blondin and Haydn
427 Thomas. Furthermore, we would like to thank Tom Wade and Simon Gibson-Poole from the
428 University of Edinburgh Airborne GeoSciences Facility, as well as Chris McLellan and
429 Andrew Gray from the NERC Field Spectroscopy Facility for their support in our drone
430 endeavours. We also want to express our gratitude to Ally Phillimore, Ed Midchard and Toke
431 Høye for providing feedback on earlier versions of this manuscript.

432

433 We thank the Herschel Island - Qikiqtaruk Territorial Park Team and Yukon Government for
434 providing logistical support for our field research on Qikiqtaruk including: Richard Gordon,
435 Cameron Eckert and the park rangers Edward McLeod, Sam McLeod, Ricky Joe, Paden
436 Lennie and Shane Goosen. We thank the research group of Hugues Lantuit at the Alfred
437 Wegener Institute and the Aurora Research Institute for logistical support. Research permits
438 include Yukon Researcher and Explorer permits (16-48S&E and 17-42S&E) and Yukon
439 Parks Research permits (RE-Inu-02-16 and 17-RE-HI-02). All airborne activities were
440 licensed under the Transport Canada special flight operations certificates ATS
441 16-17-00008441 RDIMS 11956834 (2016) and ATS 16-17-00072213 RDIMS 12929481
442 (2017).

443

444 Funding for this research was provided by NERC through the ShrubTundra standard grant
445 (NE/M016323/1), a NERC E3 Doctoral Training Partnership PhD studentship for Jakob
446 Assmann (NE/L002558/1), a research grant from the National Geographic Society
447 (CP-061R-17), a Parrot Climate Innovation Grant, the Aarhus University Research
448 Foundation, and the European Union's Horizon 2020 research and innovation programme
449 under the Marie Skłodowska-Curie grant agreement (754513) for Jeffrey Kerby, a NERC
450 support case for use of the NERC Field Spectroscopy Facility (738.1115), equipment loans
451 from the University of Edinburgh Airborne GeoSciences Facility and the NERC Geophysical
452 Equipment Facility (GEF 1063 and 1069).

453

454 Finally, we would like to thank the Inuvialuit people for the opportunity to conduct research in
455 the Inuvialuit Settlement Region.

456

457 **Author Contributions**

458

459 JJA and IMS conceived the study with input from JTK and AMC. JJA carried out data
460 processing and analysis. JJA and IMS led the drone and ground-validation field work in

461 2016. AMC led the drone field surveys with input from JTK and GD led the ground-validation
462 for 2017 with input from JTK. JJA, IMS and JTK wrote the manuscript with input from AMC
463 and GD. IMS supervised and acquired funding for the research.

464

465 **Data availability**

466

467 All processed drone and Sentinel imagery is available via a data repository on Zenodo
468 (embargoed till publication of this manuscript).

469 Should the reviewers wish to access the data prior publication, a mirror of the Zenodo
470 repository can be accessed via this confidential link:

471 -

472

473 All code used to conduct the analysis, produce figures and as well as summary data
474 outputs and MODIS pixel values can be found on this GitHub repository (already openly
475 available):

476 https://github.com/jakobjassmann/qhi_phen_ts

477

478 **References**

479

- 480 1. Levin SA. The Problem of Pattern and Scale in Ecology: The Robert H. MacArthur
481 Award Lecture. *Ecology*. 1992 Dec 1;73(6):1943–67.
- 482 2. Anderson CB. Biodiversity monitoring, earth observations and the ecology of scale.
483 *Ecol Lett*. 2018 Oct 1;21(10):1572–85.
- 484 3. Estes L, Elsen PR, Treuer T, Ahmed L, Caylor K, Chang J, et al. The spatial and
485 temporal domains of modern ecology. *Nat Ecol Evol*. 2018 May;2(5):819.
- 486 4. Chapin FS, Sturm M, Serreze MC, McFadden JP, Key JR, Lloyd AH, et al. Role of
487 land-surface changes in arctic summer warming. *Science*. 2005 Oct
488 28;310(5748):657–60.
- 489 5. Loranty MM, Goetz SJ. Shrub expansion and climate feedbacks in Arctic tundra.
490 *Environ Res Lett*. 2012 Mar 1;7(1):011005.
- 491 6. Pearson RG, Phillips SJ, Loranty MM, Beck PSA, Damoulas T, Knight SJ, et al. Shifts
492 in Arctic vegetation and associated feedbacks under climate change. *Nat Clim Change*.
493 2013 Jul;3(7):673–7.
- 494 7. Richardson AD, Keenan TF, Migliavacca M, Ryu Y, Sonnentag O, Toomey M. Climate
495 change, phenology, and phenological control of vegetation feedbacks to the climate
496 system. *Agric For Meteorol*. 2013 Feb 15;169:156–73.
- 497 8. Ernakovich JG, Hopping KA, Berdanier AB, Simpson RT, Kachergis EJ, Steltzer H, et
498 al. Predicted responses of arctic and alpine ecosystems to altered seasonality under
499 climate change. *Glob Change Biol* [Internet]. 2014 Mar 1 [cited 2014 Apr 9]; Available
500 from: <http://onlinelibrary.wiley.com/doi/10.1111/gcb.12568/abstract>
- 501 9. Diepstraten RAE, Jessen TD, Fauvelle CMD, Musiani MM. Does climate change and
502 plant phenology research neglect the Arctic tundra? *Ecosphere*. 2018;9(9):e02362.
- 503 10. Metcalfe DB, Hermans TDG, Ahlstrand J, Becker M, Berggren M, Björk RG, et al.
504 Patchy field sampling biases understanding of climate change impacts across the
505 Arctic. *Nat Ecol Evol*. 2018 Sep;2(9):1443.
- 506 11. Beamish A, Raynolds MK, Epstein H, Frost GV, Macander MJ, Bergstedt H, et al.
507 Recent trends and remaining challenges for optical remote sensing of Arctic tundra
508 vegetation: A review and outlook. *Remote Sens Environ*. 2020 Sep 1;246:111872.
- 509 12. Stoy PC, Williams M, Disney M, Prieto-Blanco A, Huntley B, Baxter R, et al. Upscaling
510 as ecological information transfer: a simple framework with application to Arctic
511 ecosystem carbon exchange. *Landsc Ecol*. 2009 Aug 1;24(7):971–86.
- 512 13. Myers-Smith IH, Kerby JT, Phoenix GK, Bjerke JW, Epstein HE, Assmann JJ, et al.
513 Complexity revealed in the greening of the Arctic. *Nat Clim Change*. 2020
514 Feb;10(2):106–17.
- 515 14. Siewert MB, Olofsson J. Scale-dependency of Arctic ecosystem properties revealed by
516 UAV. *Environ Res Lett* [Internet]. 2020 Jul 2 [cited 2020 Jul 6]; Available from:
517 <https://iopscience.iop.org/article/10.1088/1748-9326/aba20b>
- 518 15. Myneni RB, Keeling CD, Tucker CJ, Asrar G, Nemani RR. Increased plant growth in the
519 northern high latitudes from 1981 to 1991. *Nature*. 1997 Apr;386(6626):698–702.
- 520 16. Tucker CJ, Slayback DA, Pinzon JE, Los SO, Myneni RB, Taylor MG. Higher northern
521 latitude normalized difference vegetation index and growing season trends from 1982
522 to 1999. *Int J Biometeorol*. 2001 Nov 1;45(4):184–90.
- 523 17. Bhatt US, Walker DA, Raynolds MK, Comiso JC, Epstein HE, Jia GJ, et al. Circumpolar
524 arctic tundra vegetation change is linked to sea ice decline. *Earth Interact*. 2010
525 Aug;14(8):1–20.
- 526 18. Guay KC, Beck PSA, Berner LT, Goetz SJ, Baccini A, Buermann W. Vegetation
527 productivity patterns at high northern latitudes: a multi-sensor satellite data
528 assessment. *Glob Change Biol*. 2014;20(10):3147–3158.

- 529 19. Zhu Z, Piao S, Myneni RB, Huang M, Zeng Z, Canadell JG, et al. Greening of the Earth
530 and its drivers. *Nat Clim Change*. 2016 Aug;6(8):791–5.
- 531 20. Keenan TF, Riley WJ. Greening of the land surface in the world's cold regions
532 consistent with recent warming. *Nat Clim Change*. 2018 Sep;8(9):825–8.
- 533 21. Zeng H, Jia G, Epstein H. Recent changes in phenology over the northern high
534 latitudes detected from multi-satellite data. *Environ Res Lett*. 2011;6(4):045508.
- 535 22. Zeng H, Jia G, Forbes BC. Shifts in Arctic phenology in response to climate and
536 anthropogenic factors as detected from multiple satellite time series. *Environ Res Lett*.
537 2013;8(3):035036.
- 538 23. Zhao J, Zhang H, Zhang Z, Guo X, Li X, Chen C. Spatial and Temporal Changes in
539 Vegetation Phenology at Middle and High Latitudes of the Northern Hemisphere over
540 the Past Three Decades. *Remote Sens*. 2015 Aug;7(8):10973–95.
- 541 24. Potter C, Alexander O. Changes in Vegetation Phenology and Productivity in Alaska
542 Over the Past Two Decades. *Remote Sens*. 2020 Jan;12(10):1546.
- 543 25. Tucker CJ. Red and photographic infrared linear combinations for monitoring
544 vegetation. *Remote Sens Environ*. 1979 May 1;8(2):127–50.
- 545 26. Myneni RB, Tucker CJ, Asrar G, Keeling CD. Interannual variations in satellite-sensed
546 vegetation index data from 1981 to 1991. *J Geophys Res Atmospheres*.
547 1998;103(D6):6145–60.
- 548 27. Elmendorf SC, Henry GHR, Hollister RD, Björk RG, Boulanger-Lapointe N, Cooper EJ,
549 et al. Plot-scale evidence of tundra vegetation change and links to recent summer
550 warming. *Nat Clim Change*. 2012 Apr 8;2:453–7.
- 551 28. Tape KD, Sturm M, Racine CH. The evidence for shrub expansion in Northern Alaska
552 and the Pan-Arctic. *Glob Change Biol*. 2006 Apr;12(4):686–702.
- 553 29. Myers-Smith IH, Forbes BC, Wilmsking M, Hallinger M, Lantz T, Blok D, et al. Shrub
554 expansion in tundra ecosystems: dynamics, impacts and research priorities. *Environ*
555 *Res Lett*. 2011 Dec 1;6(4):045509.
- 556 30. Tape K, Hallinger M, Welker J, Ruess R. Landscape heterogeneity of shrub expansion
557 in Arctic Alaska. *Ecosystems*. 2012;15(5):711–24.
- 558 31. García Criado M, Myers-Smith IH, Bjorkman AD, Lehmann CER, Stevens N. Woody
559 plant encroachment intensifies under climate change across tundra and savanna
560 biomes. *Glob Ecol Biogeogr*. 2020;(in press).
- 561 32. Bjorkman AD, Myers-Smith IH, Elmendorf SC, Normand S, R ger N, Beck PSA, et al.
562 Plant functional trait change across a warming tundra biome. *Nature*. 2018
563 Oct;562(7725):57–62.
- 564 33. H ye TT, Post E, Meltofte H, Schmidt NM, Forchhammer MC. Rapid advancement of
565 spring in the High Arctic. *Curr Biol*. 2007 Jun 19;17(12):R449–51.
- 566 34. Kerby JT, Post E. Advancing plant phenology and reduced herbivore production in a
567 terrestrial system associated with sea ice decline. *Nat Commun [Internet]*. 2013 Oct 1
568 [cited 2014 Oct 23];4. Available from:
569 [http://www.nature.com/ncomms/2013/131001/ncomms3514/full/ncomms3514.html?me](http://www.nature.com/ncomms/2013/131001/ncomms3514/full/ncomms3514.html?message-global=remove)
570 [ssage-global=remove](http://www.nature.com/ncomms/2013/131001/ncomms3514/full/ncomms3514.html?message-global=remove)
- 571 35. Post E, Kerby J, Pedersen C, Steltzer H. Highly individualistic rates of plant
572 phenological advance associated with arctic sea ice dynamics. *Biol Lett*. 2016 Dec
573 1;12(12):20160332.
- 574 36. Assmann JJ, Myers-Smith IH, Phillimore AB, Bjorkman AD, Ennos RE, Prev y JS, et
575 al. Local snow melt and temperature—but not regional sea ice—explain variation in
576 spring phenology in coastal Arctic tundra. *Glob Change Biol*. 2019;25(7):2258–74.
- 577 37. Oberbauer SF, Elmendorf SC, Troxler TG, Hollister RD, Rocha AV, Bret-Harte MS, et
578 al. Phenological response of tundra plants to background climate variation tested using
579 the International Tundra Experiment. *Philos Trans R Soc B Biol Sci [Internet]*. 2013 Aug

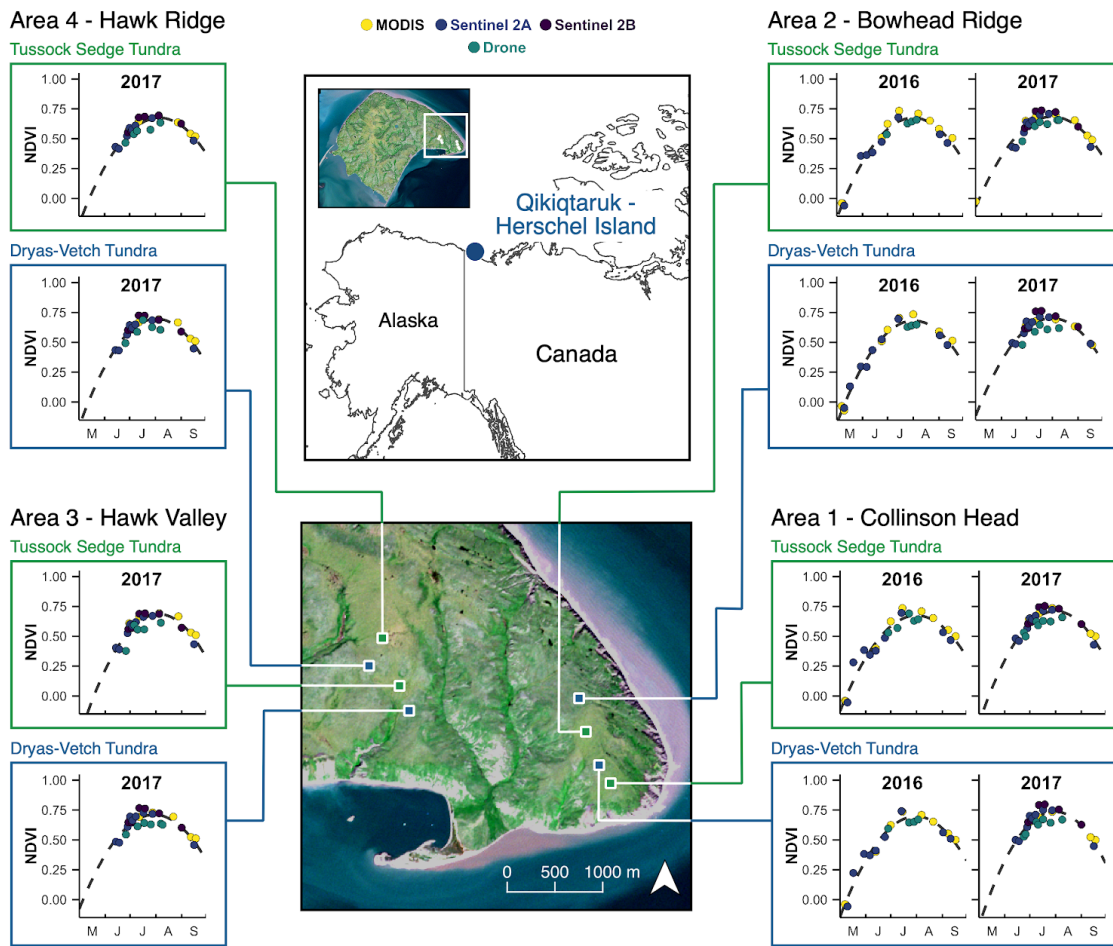
- 580 19 [cited 2013 Aug 20];368(1624). Available from:
581 <http://rstb.royalsocietypublishing.org/content/368/1624/20120481>
- 582 38. Bjorkman AD, Elmendorf SC, Beamish AL, Vellend M, Henry GHR. Contrasting effects
583 of warming and increased snowfall on Arctic tundra plant phenology over the past two
584 decades. *Glob Change Biol*. 2015 Dec 1;21(12):4651–61.
- 585 39. Prev y JS, Rixen C, R ger N, H ye TT, Bjorkman AD, Myers-Smith IH, et al. Warming
586 shortens flowering seasons of tundra plant communities. *Nat Ecol Evol*. 2019
587 Jan;3(1):45.
- 588 40. Jia GJ, Epstein HE, Walker DA. Spatial heterogeneity of tundra vegetation response to
589 recent temperature changes. *Glob Change Biol*. 2006 Jan;12(1):42–55.
- 590 41. Raynolds MK, Comiso JC, Walker DA, Verbyla D. Relationship between
591 satellite-derived land surface temperatures, arctic vegetation types, and NDVI. *Remote
592 Sens Environ*. 2008 Apr 15;112(4):1884–94.
- 593 42. Jia GJ, Epstein HE, Walker DA. Vegetation greening in the Canadian Arctic related to
594 decadal warming. *J Environ Monit*. 2009;11(12):2231.
- 595 43. Bhatt US, Walker DA, Raynolds MK, Bieniek PA, Epstein HE, Comiso JC, et al. Recent
596 declines in warming and vegetation greening trends over Pan-Arctic tundra. *Remote
597 Sens*. 2013 Aug 29;5(9):4229–54.
- 598 44. Xu L, Myneni RB, Chapin Iii FS, Callaghan TV, Pinzon JE, Tucker CJ, et al.
599 Temperature and vegetation seasonality diminishment over northern lands. *Nat Clim
600 Change* [Internet]. 2013 Mar 10 [cited 2013 Mar 12]; Available from:
601 <http://www.nature.com/nclimate/journal/vaop/ncurrent/full/nclimate1836.html>
- 602 45. Piao S, Nan H, Huntingford C, Ciais P, Friedlingstein P, Sitch S, et al. Evidence for a
603 weakening relationship between interannual temperature variability and northern
604 vegetation activity. *Nat Commun*. 2014 Oct 16;5:5018.
- 605 46. Vickers H, H gda KA, Solb  S, Karlsen SR, T mmervik H, Aanes R, et al. Changes in
606 greening in the high Arctic: insights from a 30 year AVHRR max NDVI dataset for
607 Svalbard. *Environ Res Lett*. 2016;11(10):105004.
- 608 47. Walker DA, Leibman MO, Epstein HE, Forbes BC, Bhatt US, Raynolds MK, et al.
609 Spatial and temporal patterns of greenness on the Yamal Peninsula, Russia:
610 interactions of ecological and social factors affecting the Arctic normalized difference
611 vegetation index. *Environ Res Lett*. 2009 Oct;4(4):045004.
- 612 48. Macias-Fauria M, Forbes BC, Zetterberg P, Kumpula T. Eurasian Arctic greening
613 reveals teleconnections and the potential for structurally novel ecosystems. *Nat Clim
614 Change*. 2012;2:613–618.
- 615 49. Post E. Erosion of community diversity and stability by herbivore removal under
616 warming. *Proc R Soc B Biol Sci*. 2013 Apr 22;280(1757):20122722.
- 617 50. Bhatt US, Walker DA, Walsh JE, Carmack EC, Frey KE, Meier WN, et al. Implications
618 of Arctic sea ice decline for the Earth system. *Annu Rev Environ Resour*.
619 2014;39:57–89.
- 620 51. Fauchald P, Park T, T mmervik H, Myneni R, Hausner VH. Arctic greening from
621 warming promotes declines in caribou populations. *Sci Adv*. 2017 Apr 1;3(4):e1601365.
- 622 52. Elmendorf SC, Henry GHR, Hollister RD, Fosaa AM, Gould WA, Hermanutz L, et al.
623 Experiment, monitoring, and gradient methods used to infer climate change effects on
624 plant communities yield consistent patterns. *Proc Natl Acad Sci*. 2015 Jan
625 13;112(2):448–52.
- 626 53. Pattison RR, Jorgenson JC, Raynolds MK, Welker JM. Trends in NDVI and tundra
627 community composition in the Arctic of NE Alaska between 1984 and 2009.
628 *Ecosystems*. 2015 Mar 19;18(4):707–19.
- 629 54. Piao S, Tan J, Chen A, Fu YH, Ciais P, Liu Q, et al. Leaf onset in the northern
630 hemisphere triggered by daytime temperature. *Nat Commun*. 2015 Apr 23;6:6911.

- 631 55. Liu Q, Fu YH, Zhu Z, Liu Y, Liu Z, Huang M, et al. Delayed autumn phenology in the
632 Northern Hemisphere is related to change in both climate and spring phenology. *Glob*
633 *Change Biol.* 2016 Nov 1;22(11):3702–11.
- 634 56. Semenchuk PR, Gillespie MAK, Rumpf SB, Baggesen N, Elberling B, Cooper EJ. High
635 Arctic plant phenology is determined by snowmelt patterns but duration of phenological
636 periods is fixed: an example of periodicity. *Environ Res Lett.* 2016;11(12):125006.
- 637 57. Prevéy J, Vellend M, Rüger N, Hollister RD, Bjorkman AD, Myers-Smith IH, et al.
638 Greater temperature sensitivity of plant phenology at colder sites: implications for
639 convergence across northern latitudes. *Glob Change Biol [Internet]*. 2017 Feb 1 [cited
640 2017 Feb 6]; Available from:
641 <http://onlinelibrary.wiley.com.ezproxy.is.ed.ac.uk/doi/10.1111/gcb.13619/abstract>
- 642 58. Jia GJ, Epstein HE, Walker DA. Greening of arctic Alaska, 1981–2001. *Geophys Res*
643 *Lett.* 2003 Oct 29;30(20):HLS 3-1.
- 644 59. Fraser RH, Olthof I, Carrière M, Deschamps A, Pouliot D. Detecting long-term changes
645 to vegetation in northern Canada using the Landsat satellite image archive. *Environ*
646 *Res Lett.* 2011 Oct 1;6(4):045502.
- 647 60. Ju J, Masek JG. The vegetation greenness trend in Canada and US Alaska from
648 1984–2012 Landsat data. *Remote Sens Environ.* 2016 Apr;176:1–16.
- 649 61. Reynolds MK, Walker DA, Verbyla D, Munger CA. Patterns of Change within a Tundra
650 Landscape: 22-year Landsat NDVI Trends in an Area of the Northern Foothills of the
651 Brooks Range, Alaska. *Arct Antarct Alp Res.* 2013 May 1;45(2):249–60.
- 652 62. Miles VV, Esau I. Spatial heterogeneity of greening and browning between and within
653 bioclimatic zones in northern West Siberia. *Environ Res Lett.* 2016;11(11):115002.
- 654 63. Lara MJ, Nitze I, Grosse G, Martin P, McGuire AD. Reduced arctic tundra productivity
655 linked with landform and climate change interactions. *Sci Rep.* 2018 Feb 5;8(1):2345.
- 656 64. Thompson JA, Koenig LS. Vegetation phenology in Greenland and links to cryospheric
657 change. *Ann Glaciol.* 2018 Dec;59(77):59–68.
- 658 65. Phoenix GK, Bjerke JW. Arctic browning: extreme events and trends reversing arctic
659 greening. *Glob Change Biol.* 2016 Sep 1;22(9):2960–2.
- 660 66. National Academies of Sciences E. Understanding Northern Latitude Vegetation
661 Greening and Browning: Proceedings of a Workshop [Internet]. 2019 [cited 2019 Oct
662 21]. Available from:
663 <https://www.nap.edu/catalog/25423/understanding-northern-latitude-vegetation-greening-and-browning-proceedings-of-a>
- 664 67. Frost GV, Bhatt US, Epstein HE, Walker DA, Reynolds MK, Berner LT, et al. Arctic
665 Report Card: Update for 2019 - Tundra Greenness [Internet]. Arctic Program. 2019
666 [cited 2019 Feb 23]. Available from:
667 <http://www.arctic.noaa.gov/Report-Card/Report-Card-2015/ArtMID/5037/ArticleID/221/Tundra-Greenness>
- 670 68. Blok D, Schaepman-Strub G, Bartholomeus H, Heijmans MMPD, Maximov TC,
671 Berendse F. The response of Arctic vegetation to the summer climate: relation between
672 shrub cover, NDVI, surface albedo and temperature. *Environ Res Lett.* 2011 Jul
673 1;6:035502.
- 674 69. Reynolds MK, Walker DA, Epstein HE, Pinzon JE, Tucker CJ. A new estimate of
675 tundra-biome phytomass from trans-Arctic field data and AVHRR NDVI. *Remote Sens*
676 *Lett.* 2012 Sep 1;3(5):403–11.
- 677 70. Berner LT, Jantz P, Tape KD, Goetz SJ. Tundra plant above-ground biomass and shrub
678 dominance mapped across the North Slope of Alaska. *Environ Res Lett.* 2018
679 Feb;13(3):035002.
- 680 71. Cunliffe AM, Assmann JJ, Daskalova G, Kerby JT, Myers-Smith IH. Aboveground
681 biomass corresponds strongly with drone-derived canopy height but weakly with

- 682 greenness (NDVI) in a shrub tundra landscape. *Environ Res Lett* [Internet]. 2020 [cited
683 2020 Jul 10]; Available from: <http://iopscience.iop.org/10.1088/1748-9326/aba470>
- 684 72. Stow D. Remote sensing of vegetation and land-cover change in arctic tundra
685 ecosystems. *Remote Sens Environ*. 2004 Feb;89(3):281–308.
- 686 73. Bartsch A, Widhalm B, Leibman M, Ermokhina K, Kumpula T, Skarin A, et al. Feasibility
687 of tundra vegetation height retrieval from Sentinel-1 and Sentinel-2 data. *Remote Sens*
688 *Environ*. 2020 Feb 1;237:111515.
- 689 74. Woodcock CE, Strahler AH. The factor of scale in remote sensing. *Remote Sens*
690 *Environ*. 1987 Apr 1;21(3):311–32.
- 691 75. Henry GHR, Molau U. Tundra plants and climate change: the International Tundra
692 Experiment (ITEX). *Glob Change Biol*. 1997 Dec 1;3(S1):1–9.
- 693 76. Beck PSA, Jönsson P, Høgda K-A, Karlsen SR, Eklundh L, Skidmore AK. A
694 ground-validated NDVI dataset for monitoring vegetation dynamics and mapping
695 phenology in Fennoscandia and the Kola peninsula. *Int J Remote Sens*. 2007 Oct
696 10;28(19):4311–30.
- 697 77. Gamon JA, Huemmrich KF, Stone RS, Tweedie CE. Spatial and temporal variation in
698 primary productivity (NDVI) of coastal Alaskan tundra: Decreased vegetation growth
699 following earlier snowmelt. *Remote Sens Environ*. 2013 Feb 15;129:144–53.
- 700 78. Kerby JT. Phenology in a changing Arctic: Linking trophic interactions across scales.
701 2015 Sep 14 [cited 2018 Oct 19]; Available from:
702 <https://etda.libraries.psu.edu/catalog/26992>
- 703 79. Anderson K, Gaston KJ. Lightweight unmanned aerial vehicles will revolutionize spatial
704 ecology. *Front Ecol Environ*. 2013 Mar 18;11(3):138–46.
- 705 80. Klosterman S, Richardson AD. Observing Spring and Fall Phenology in a Deciduous
706 Forest with Aerial Drone Imagery. *Sensors*. 2017 Dec;17(12):2852.
- 707 81. Assmann JJ, Kerby JT, Cunliffe AM, Myers-Smith IH. Vegetation monitoring using
708 multispectral sensors — best practices and lessons learned from high latitudes. *J*
709 *Unmanned Veh Syst*. 2018 Dec 5;7(1):54–75.
- 710 82. Klosterman S, Hufkens K, Richardson AD. Later springs green-up faster: the relation
711 between onset and completion of green-up in deciduous forests of North America. *Int J*
712 *Biometeorol*. 2018 Sep 1;62(9):1645–55.
- 713 83. Myers-Smith IH, Hik DS. Shrub canopies influence soil temperatures but not nutrient
714 dynamics: An experimental test of tundra snow–shrub interactions. *Ecol Evol*. 2013 Oct
715 1;3(11):3683–700.
- 716 84. Smith C, Kennedy C, Hargrave A, McKenna K. Soil and Vegetation of Herschel Island.
717 Whitehorse, Yukon Territory, Canada: Agriculture Canada; 1989. Report No.: No 1.
- 718 85. Obu J, Lantuit H, Myers-Smith I, Heim B, Wolter J, Fritz M. Effect of Terrain
719 Characteristics on Soil Organic Carbon and Total Nitrogen Stocks in Soils of Herschel
720 Island, Western Canadian Arctic. *Permafrost Periglacial Process*. 2015 Jan 1;28(1):92–107.
- 721 86. Didan K. MOD13Q1 MODIS/Terra Vegetation Indices 16-Day L3 Global 250m SIN Grid
722 V006 [Internet]. NASA EOSDIS Land Processes DAAC; 2015 [cited 2018 Oct 22].
723 Available from: <https://doi.org/10.5067/MODIS/MOD13Q1.006>
- 724 87. Gorelick N, Hancher M, Dixon M, Ilyushchenko S, Thau D, Moore R. Google Earth
725 Engine: Planetary-scale geospatial analysis for everyone. *Remote Sens Environ*. 2017
726 Dec 1;202:18–27.
- 727 88. Mueller-Wilm U. Sen2Cor Software Release Note: Ref.:
728 S2-PDGS-MPC-L2A-SRN-V2.4.0 [Internet]. 2017 [cited 2018 Oct 22]. Available from:
729 [http://step.esa.int/thirdparties/sen2cor/2.4.0/Sen2Cor_240_Documentation_PDF/S2-PD](http://step.esa.int/thirdparties/sen2cor/2.4.0/Sen2Cor_240_Documentation_PDF/S2-PDGS-MPC-L2A-SRN-V2.4.0.pdf)
730 [GS-MPC-L2A-SRN-V2.4.0.pdf](http://step.esa.int/thirdparties/sen2cor/2.4.0/Sen2Cor_240_Documentation_PDF/S2-PDGS-MPC-L2A-SRN-V2.4.0.pdf)
- 731 89. Molau U, Mølgaard P. International Tundra Experiment Manual [Internet]. 1996.
732 Available from: <https://www.gvsu.edu/itex/library-8.htm>

- 733 90. R Core Team. R: A language and environment for statistical computing. R Foundation
734 for Statistical Computing, Vienna, Austria. 2013. 2014.
- 735 91. Hijmans RJ, Etten J van, Sumner M, Cheng J, Baston D, Bevan A, et al. raster:
736 Geographic Data Analysis and Modeling [Internet]. 2020 [cited 2020 Jul 11]. Available
737 from: <https://CRAN.R-project.org/package=raster>
- 738 92. Fernández-Guisuraga JM, Sanz-Ablanedo E, Suárez-Seoane S, Calvo L. Using
739 Unmanned Aerial Vehicles in Postfire Vegetation Survey Campaigns through Large and
740 Heterogeneous Areas: Opportunities and Challenges. *Sensors*. 2018 Feb;18(2):586.
- 741 93. Fawcett D, Panigada C, Tagliabue G, Boschetti M, Celesti M, Evdokimov A, et al.
742 Multi-Scale Evaluation of Drone-Based Multispectral Surface Reflectance and
743 Vegetation Indices in Operational Conditions. *Remote Sens*. 2020 Jan;12(3):514.
- 744 94. Matese A, Toscano P, Di Gennaro SF, Genesisio L, Vaccari FP, Primicerio J, et al.
745 Intercomparison of UAV, Aircraft and Satellite Remote Sensing Platforms for Precision
746 Viticulture. *Remote Sens*. 2015 Mar;7(3):2971–90.
- 747 95. Franzini M, Ronchetti G, Sona G, Casella V. Geometric and Radiometric Consistency
748 of Parrot Sequoia Multispectral Imagery for Precision Agriculture Applications. *Appl Sci*.
749 2019 Jan;9(24):5314.
- 750 96. Khaliq A, Comba L, Biglia A, Ricauda Aimonino D, Chiaberge M, Gay P. Comparison of
751 Satellite and UAV-Based Multispectral Imagery for Vineyard Variability Assessment.
752 *Remote Sens*. 2019 Jan;11(4):436.
- 753 97. Stoy PC, Williams M, Spadavecchia L, Bell RA, Prieto-Blanco A, Evans JG, et al. Using
754 Information Theory to Determine Optimum Pixel Size and Shape for Ecological Studies:
755 Aggregating Land Surface Characteristics in Arctic Ecosystems. *Ecosystems*. 2009 Jun
756 1;12(4):574–89.
- 757 98. Virtanen T, Ek M. The fragmented nature of tundra landscape. *Int J Appl Earth Obs*
758 *Geoinformation*. 2014 Apr 1;27:4–12.
- 759 99. Myers–Smith IH, Grabowski MM, Thomas HJD, Angers–Blondin S, Daskalova GN,
760 Bjorkman AD, et al. Eighteen years of ecological monitoring reveals multiple lines of
761 evidence for tundra vegetation change. *Ecol Monogr*. 2019;89(2):e01351.
- 762 100. Høye TT, Post E, Schmidt NM, Trøjelsgaard K, Forchhammer MC. Shorter flowering
763 seasons and declining abundance of flower visitors in a warmer Arctic. *Nat Clim*
764 *Change*. 2013 Aug;3(8):759–63.
- 765 101. Armstrong JB, Takimoto G, Schindler DE, Hayes MM, Kauffman MJ. Resource waves:
766 phenological diversity enhances foraging opportunities for mobile consumers. *Ecology*.
767 2016;97(5):1099–112.
- 768 102. Miller CE, Griffith PC, Goetz SJ, Hoy EE, Pinto N, McCubbin IB, et al. An overview of
769 ABoVE airborne campaign data acquisitions and science opportunities. *Environ Res*
770 *Lett*. 2019 Jul;14(8):080201.
- 771 103. Klosterman S, Melaas E, Wang JA, Martinez A, Frederick S, O’Keefe J, et al.
772 Fine-scale perspectives on landscape phenology from unmanned aerial vehicle (UAV)
773 photography. *Agric For Meteorol*. 2018 Jan 15;248:397–407.
- 774 104. Berra EF, Gaulton R, Barr S. Assessing spring phenology of a temperate woodland: A
775 multiscale comparison of ground, unmanned aerial vehicle and Landsat satellite
776 observations. *Remote Sens Environ*. 2019 Mar 15;223:229–42.
- 777 105. D’Odorico P, Besik A, Wong CYS, Isabel N, Ensminger I. High-throughput drone-based
778 remote sensing reliably tracks phenology in thousands of conifer seedlings. *New*
779 *Phytol*. 2020;226(6):1667–81.
- 780 106. Prevéy J, Vellend M, Rüger N, Hollister RD, Bjorkman AD, Myers–Smith IH, et al.
781 Greater temperature sensitivity of plant phenology at colder sites: implications for
782 convergence across northern latitudes. *Glob Change Biol*. 2017;23(7):2660–71.
- 783 107. Fawcett D, Anderson K. Investigating impacts of calibration methodology and

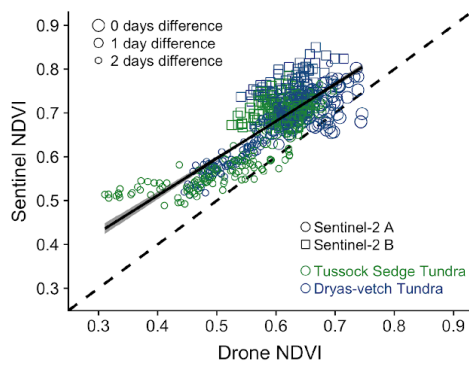
784 irradiance variations on lightweight drone-based sensor derived surface reflectance
785 products. In: Remote Sensing for Agriculture, Ecosystems, and Hydrology XXI
786 [Internet]. International Society for Optics and Photonics; 2019 [cited 2020 Jul 11]. p.
787 111490D. Available from:
788 <https://www.spiedigitallibrary.org/conference-proceedings-of-spie/11149/111490D/Investigating-impacts-of-calibration-methodology-and-irradiance-variations-on-lightweight/10.1117/12.2533106.short>
789
790
791 108. Huang S, Tang L, Hupy JP, Wang Y, Shao G. A commentary review on the use of
792 normalized difference vegetation index (NDVI) in the era of popular remote sensing. *J*
793 *For Res* [Internet]. 2020 May 31 [cited 2020 Jul 11]; Available from:
794 <https://doi.org/10.1007/s11676-020-01155-1>
795 109. Zhang Q, Yao T, Huemmrich KF, Middleton EM, Lyapustin A, Wang Y. Evaluating
796 impacts of snow, surface water, soil and vegetation on empirical vegetation and snow
797 indices for the Utqiagvik tundra ecosystem in Alaska with the LVS3 model. *Remote*
798 *Sens Environ*. 2020 Apr 1;240:111677.
799 110. Aasen H, Honkavaara E, Lucieer A, Zarco-Tejada PJ. Quantitative Remote Sensing at
800 Ultra-High Resolution with UAV Spectroscopy: A Review of Sensor Technology,
801 Measurement Procedures, and Data Correction Workflows. *Remote Sens*. 2018
802 Jul;10(7):1091.
803 111. Post E, Alley RB, Christensen TR, Macias-Fauria M, Forbes BC, Gooseff MN, et al.
804 The polar regions in a 2°C warmer world. *Sci Adv*. 2019 Dec 1;5(12):eaaw9883.
805 112. Strahler AH, Woodcock CE, Smith JA. On the nature of models in remote sensing.
806 *Remote Sens Environ*. 1986 Oct 1;20(2):121–39.
807 113. Chen JM. Spatial Scaling of a Remotely Sensed Surface Parameter by Contexture.
808 *Remote Sens Environ*. 1999 Jul 1;69(1):30–42.
809 114. Chen JM, Chen X, Ju W. Effects of vegetation heterogeneity and surface topography
810 on spatial scaling of net primary productivity. *Biogeosciences*. 2013 Jul
811 18;10(7):4879–96.
812 115. Garrigues S, Allard D, Baret F, Weiss M. Influence of landscape spatial heterogeneity
813 on the non-linear estimation of leaf area index from moderate spatial resolution remote
814 sensing data. *Remote Sens Environ*. 2006 Dec 30;105(4):286–98.
815 116. Becker RA, Wilks AR, Brownrigg R, Minka TP, Deckmyn A. maps: Draw Geographical
816 Maps [Internet]. 2018. Available from: <https://CRAN.R-project.org/package=maps>
817 117. Becker RA, Wilks AR, Brownrigg R. mapdata: Extra Map Databases [Internet]. 2018.
818 Available from: <https://CRAN.R-project.org/package=mapdata>
819



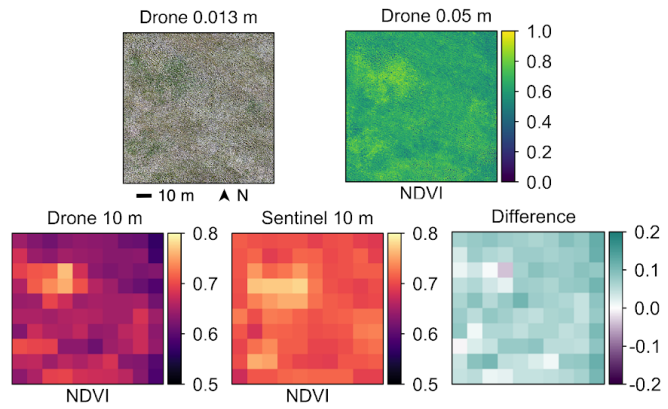
820 **Figure 1:** Drone-data captured the temporal variation in satellite data across vegetation communities, areas and
 821 years. This figure showcases variation in landscape greenness (NDVI) across the one-hectare sampling plots on
 822 Qikiqtaruk and outlines cross-season agreement amongst drone, Sentinel-2 and MODIS sensors. Map sources:
 823 North America (116,117) and Qikiqtaruk, Copernicus Sentinel-2 true colour image July 2017.

824

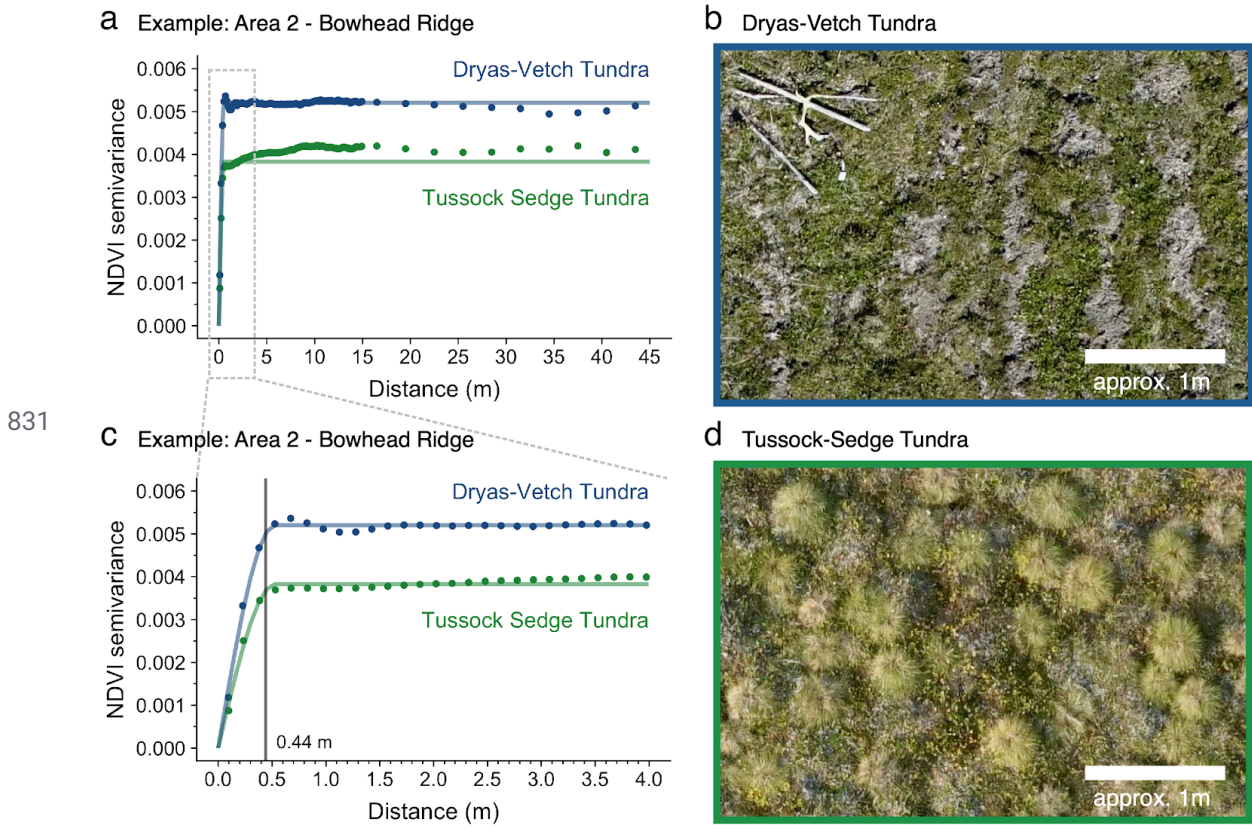
a Drone vs. Sentinel-2 NDVI



b Example: Area 2 - Dryas-vetch Tundra

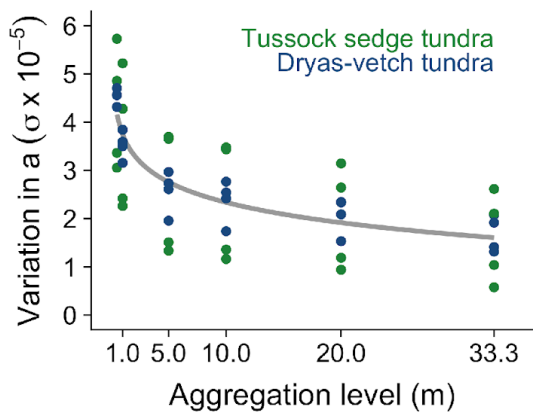


825 **Figure 2:** Drone-data better captured spatial heterogeneity in NDVI relative to Sentinel-2 MSI. a) Pixel by pixel
826 correlations between 10 m aggregated drone NDVI and native 10 m Sentinel-2 NDVI for a random sample of
827 pixels (10% of total pixels, $n = 700$) across all drone-sentinel image pairs for the 2017 growing season. b)
828 Example visualisations from the Dryas-vetch tundra at Area 2 - Bowhead Ridge showing ultra-fine-grain 0.013 m
829 true colour RGB imagery, 0.05 m native-scale drone NDVI, 10 m resampled drone NDVI, 10 m native Sentinel-2
830 NDVI and the absolute difference between resampled drone and Sentinel-2 NDVI.

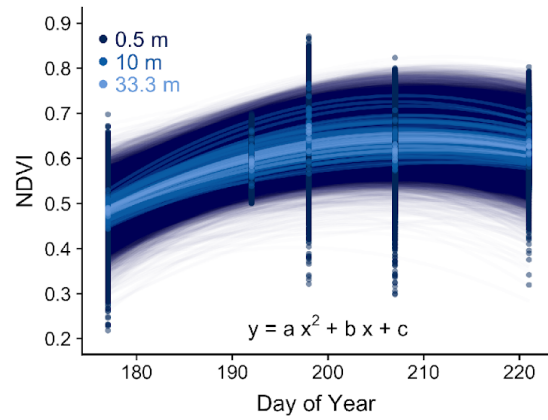


832 **Figure 3:** Spatial variation of vegetation greenness peaked at distances of ~0.5 m in both studied vegetation
 833 types, with little or no increase in the spatial dependence of greenness at distances above ~0.5 m. Figure shows
 834 example variograms. Overall spatial variation in greenness is higher in the Dryas-Vetch Tundra when compared
 835 to the Tussock-Sedge Tundra (a and c). Left panels: variograms for the Dryas-vetch and tussock sedge tundra
 836 plots in Area 2 for distances up to 5 m (a) and 45 m (c) at peak season in 2017. The dark grey line in (c) indicates
 837 the mean range estimated from the variogram models of both vegetation types from Areas 1, 2, and 4 during
 838 peak-season (26 and 28 July) in 2017 (see also Figure S1). Right panels: Dryas-vetch tundra with bare ground
 839 patches caused by cryoturbation and solifluction (c) and tussocks sedge tundra with distinctive patterns of
 840 tussocks interspersed by patches of willows and herbs (d).

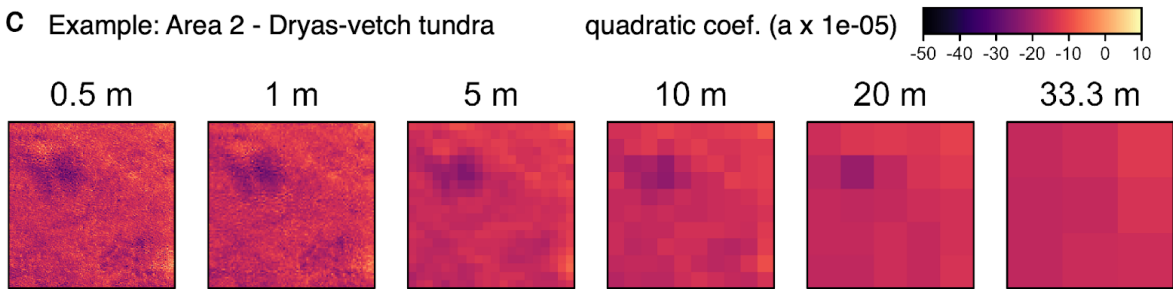
a Variation in quadratic coef. with agg. level



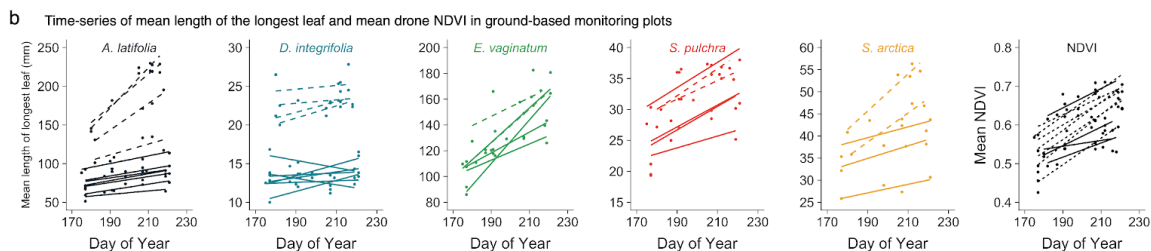
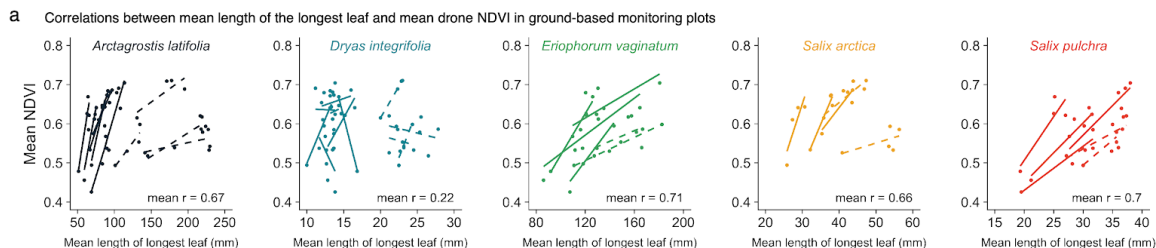
b Example curves: Area 2 - Dryas-vetch tundra



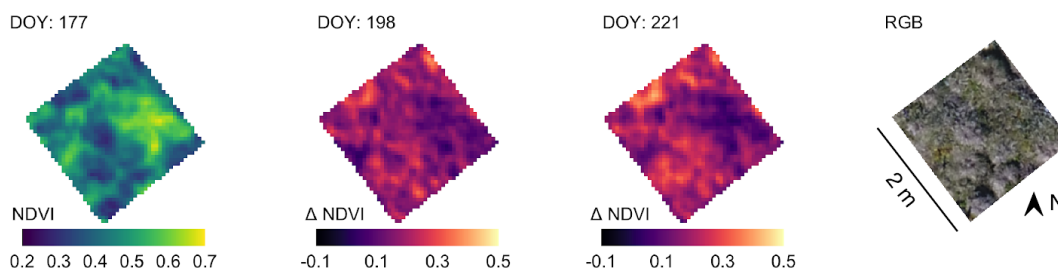
c Example: Area 2 - Dryas-vetch tundra



842 **Figure 4:** Fine-scale variation representing key ecological heterogeneity in tundra phenology was lost when
 843 aggregating from ultra-fine-grain drone to medium-grain satellite pixel sizes. When aggregating the drone data
 844 across grain sizes, we observed a logarithmic decay in variation (standard deviation) in the quadratic coefficient
 845 (shown in a) of simple growing season curves fitted to the eight vegetation plots in the 2017 season. As
 846 examples we visualise all curve-fits for the dryas-vetch tundra plot in Area 2 fitted to the time-series of the
 847 minimum, central and maximum grain-sizes tested (0.5 m, 10 m and 33.3 m) in (b) and show the spatial
 848 distribution of the quadratic coefficient for each grain size for dryas-vetch tundra plot in Area 2 in panel c), similar
 849 patterns are found across all areas (a). See Figure S7 for example curves from the dryas vetch tundra plot in
 850 Area 2 from all tested grain sizes.



c Example: Drone time-series of the ground-based monitoring plot in Area 2 - Tussock Sedge Tundra in 2017



851

852

853 **Figure 5:** Time-series of ground-based leaf length measurements correlated with drone-derived mean NDVI
 854 across four of five dominant plant species on Qikiqtaruk. Correlation between mean longest leaf length and NDVI
 855 in each 2 m x 2 m ground-phenology plot across all species, areas and seasons (a) and the corresponding
 856 time-series (b). Dashed lines indicate time-series from 2016 and solid lines indicate time-series from 2017. Lines
 857 represent least-square regressions to illustrate the relationships of longest-leaf length and NDVI (a), as well as
 858 day of year (DOY) and the time-series variable (b) for each plot and year combination. Uneven numbers of
 859 time-series between species result as the set of species monitored varied between vegetation types. (c) As an
 860 example, we illustrate the drone-based NDVI observations by showing the start, midpoint and end of the
 861 timeseries for the 2 m x 2 m ground-validation plot in the tussock sedge tundra of Area 2 in 2017. The first
 862 time-point in (c) represents the greenness in the plot at the beginning of the time-series, the two subsequent plots
 863 show the relative difference in greenness to this first observation at the given DOY, and the final plot shows a
 864 true-colour image of the plot taken by drone on the 17 July 2017 (DOY 198).